ELSEVIER

Journal of Photochemistry and Photobiology A: Chemistry 101 (1996) 75–84

Journal of PHOTOCHEMISTRY AND PHOTOBIOLOGY A: CHEMISTRY

Photochemistry in porous materials IV. Oxygen quenching of the fluorescence of fluoranthenes adsorbed on silica gel differing in pore size ☆

Christian Springob [a], Thomas Wolff [b,*]

[a] *Universität-GH-Siegen, Physikalische Chemie, D-57068 Siegen, Germany*

[b] *Technische Universität Dresden, Institut für Physikalische Chemie und Elektrochemie, D-01062 Dresden, Germany*

Received 26 February 1996; accepted 29 April 1996

Abstract

Oxygen quenching of fluoranthene and benzo[*b*]fluoranthene adsorbed on silica gels (pore size between 2.2 and 100 nm) was investigated via time-resolved and steady-state measurements. In contrast with fluorescence spectra and lifetimes, excitation spectra of adsorbed fluoranthenes were strongly altered compared with solutions. Quenching efficiencies and rate constants were found to coincide for the two fluorescers but to depend on pore size, on the surface area covered, on the presence of inert gases and in a time-dependent manner on the series order of gas addition. Since saturation of quenching occurs, the results support a Langmuir–Hinshelwood mechanism of the quenching reaction. Data evaluation yielded heats of adsorption of oxygen between 24 and 31.5 kJ mol^{-1}, higher values being found in material of small pore size.

Keywords: Porous materials; Oxygen quenching; Fluorescence; Fluoroanthenes; Silica gel

1. Introduction

The investigation of fluorescent molecules adsorbed on silica gels has a long tradition starting with the studies of Kautsky and coworkers [2,3] about 60 years ago which were the first to prove the formation of singlet oxygen. Adsorbed as well as covalently bound fluorescence probes can be employed for monitoring surface properties and dynamic processes on surfaces [4]. Still under discussion is the mechanism of fluorescence quenching by oxygen; in the literature, papers can be found in favour of quenching by coadsorbed oxygen (Langmuir–Hinshelwood mechanism [5–7]) ([7] is Part I of this series of papers) as well as of quenching directly from the gas phase (Eley–Rideal mechanism [9–11]). Also, the effects of the silica gel pore size on quenching reactions have been reported [12], and enhancement of quenching by inert gases has been described [9,10] that still awaits a convincing explanation. Additional interest in the quenching mechanism arises from possible applications of such systems to oxygen sensors [13–15].

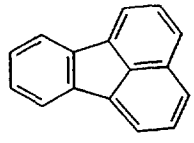

Fluoranthene

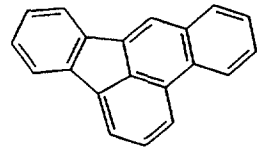

Benzo[b]fluoranthene

All these open questions prompted us to study oxygen quenching in silica gels varying in mean pore size from 2.2 to 100 nm. As fluorescent adsorbates we chose fluoranthene and benzo[*b*]fluoranthene for their comparatively long fluorescence lifetimes (50–70 ns in degassed solution [16,17]), that allow us to observe quenching over a large range of quencher concentrations. Some studies on fluoranthene can be found in the literature describing the facts that (i) in solution the fluorescence is quenched at a rate distinctly below diffusion control [16,17], (ii) excited fluoranthene does not generate singlet oxygen [18,19] and (iii) fluoranthene (being an anthropogenic compound) serves as a photosensitizer with antiviral activity in a plant [20]. Also, there has been some discussion on S_2 fluorescence in the literature [21–23].

☆ For Part III, see Ref. [1].

* Corresponding author.

PII S1010-6030(96)04397-3

2. Experimental details

2.1. Substances

Fluoranthene (Aldrich; purity 98–99%) was recrystallized three times from ethanol. Benzo[*b*]fluoranthene (Aldrich; purity 99%) was used as supplied. Data of the silica gels used are collected in Table 1. They cover microporous gels (silica gel 22), mesoporous gels (Si 40, 60, 100 and 150) and macroporous gels (Si 1000). Solvents were spectroscopic grade throughout.

2.2. Adsorption of fluoranthenes

These silica gels were dried for 24 h at 80–100 °C and at ambient pressure to remove physisorbed water but to retain silanol groups [24]. To 5 ml of dry *n*-pentane solutions containing fluoranthene or benzo[*b*]fluoranthene at known concentrations, 1 g of the respective silica gel was added, the mixture was sealed and allowed to stand for 2 days at room temperature. The solution was separated from the solid, its volume was determined and its content of (not adsorbed) aromatics was measured spectrophotometrically. Pentane left on the solid was evaporated in vacuo at room temperature. Samples thus prepared were stored in a desiccator until measurement. Another preparation method, adsorption via the gas phase [25], did not affect the results [1].

2.3. Surface coverage

The surface area Θ_F covered by fluoranthenes was calculated according to $\Theta_F = n_{ad}/n_m$, where n_{ad} (mol/g) is the amount of molecules adsorbed (determined spectrophotometrically taking into account the rest of solution left on the solid; see above) and n_m is the amount of adsorbate needed to form a monolayer. n_m is derived from $n_m = a/\sigma N_A$ with a the specific surface area of the silica gel (Table 1), σ the area occupied by an adsorbed molecule and N_A Avogadro's number. σ was estimated to be 55 Å^2 for fluoranthene and 75 Å^2 for benzo[*b*]fluoranthene. For Si 22 the specific surface area a was not available. We assume that a(Si 22) $\geq a$(Si 40) and accordingly Θ_F(Si 22) $\leq \Theta_F$(Si 40). Θ_O, the surface area covered by oxygen, was calculated from gas-kinetic expressions (see Section 4).

Table 1
Silica gels used in this study

Gel	Specific surface area [a] ($m^2\ g^{-1}$)	Mean pore diameter [b] (nm)	Supplier
Si 22	Not available	2.2	Sigma (for column chromatography)
Si 40	651	3.7	Fluka (for column chromatography)
Si 100	400	8.6	Fluka (for column chromatography)
Si 150	340	15	Aldrich (type 62)
Si 1000	20	100	Merck (LiChrospher Si 1000)

[a] According to a N_2 Brunauer–Emmett–Teller analysis by supplier.
[b] As stated by supplier.

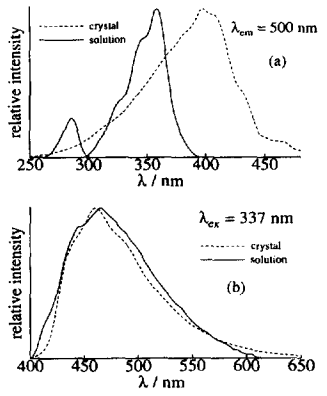

Fig. 1. (a) Excitation spectra of solid fluoranthene and of a 10^{-4} mol dm^{-3} solution of fluoranthene in ethanol. (b) Fluorescence spectra of the samples in (a).

2.4. Spectroscopic methods

UV–visible spectra were taken on Acta (M4 or M7) or Perkin–Elmer (Lambda 19) spectrometers. For measuring fluorescence spectra a Spex (Fluorolog 2) fluorometer in front-surface geometry was used. Emission spectra are corrected for photomultiplier sensitivity and for variations in the excitation light intensity; excitation spectra are uncorrected with respect to the intensity of the excitation light source. Fluorescence decay curves were measured in 1 mm cuvettes after evacuation (10^{-5} mbar for 3 h at room temperature) and, if appropriate, after subsequent filling with the desired gas mixture. To obtain decay profiles an apparatus described earlier [26] was used. This apparatus includes a nitrogen laser (emitting at 337 nm) as excitation source and it was tested by reproducing lifetimes of published systems: quinine bisulphate in 0.5 M H_2SO_4 ($\tau = 20 \pm 1$ ns [27]), 9,10-diphenylanthracene in cyclohexane ($\tau = 9 \pm 0.5$ ns [28]). All measurements were performed at room temperature.

3. Results

3.1. Spectra

Fig. 1 displays fluorescence excitation spectra of solid fluoranthene and of an ethanolic solution as well as the corresponding emission spectra. The latter appear quite similar except for the long-wavelength tail, which in the crystal case shows some increase in intensity reminescent of excimer emission. The (non-corrected) excitation spectrum in solution exhibits the same peaks and shoulders as the corresponding absorption spectrum. In the excitation spectrum of solid

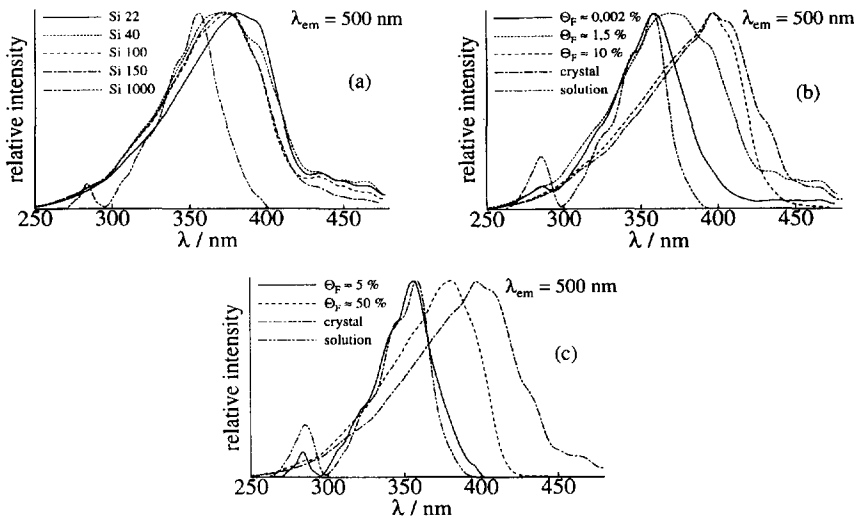

Fig. 2. Fluorescence excitation spectra of fluoranthene adsorbed (a) on various silica gels at low surface coverages (0.01–0.05), (b) on Si 40 at various surface coverages, Θ_F, compared with dissolved (10^{-4} mol dm^{-3} in ethanol) and crystalline fluoranthene and (c) on Si 1000 at two surface coverages Θ_F.

fluoranthene, however, a marked red shift is observed probably owing to intermolecular interactions in the crystal [30–33]. Adsorbed samples at low surface coverage (below 0.05) behave intermediately; as shown in Fig. 2(a), excitation spectra are red shifted except for the silica gel with the largest pore size. At small pore sizes or at high coverages, the spectra become more similar to the crystal case (Figs. 2(b) and 2(c) respectively). Corresponding but less systematic features can be obtained for benzo[*b*]fluoranthene (Fig. 3). It should be noted that the excitation and fluorescence spectra did not change when samples were stored for up to 1 year. This indicates that the adsorbed samples are in their thermodynamic equilibrium.

Fluorescence spectra of adsorbed samples appear more uniform (Fig. 4) compared with the excitation spectra. At low coverages (0.05 or less) (Fig. 4(a)) the emission of the sample with the largest pore size is almost like that in solution, resembling the excitation spectrum (Fig. 2(a)). In the other gels, some more quanta are emitted in the long-wavelength portion of the spectrum, as in the crystalline case (Fig. 1(b)). Interestingly, the high energy onsets of fluorescence are almost the same for all samples in spite of the differing excitation spectra. When the samples are excited at 450 nm, i.e. outside the absorption region of monomers in solution or in the low coverage case, only a broad long-wavelength emission is found (Fig. 5). Fluorescence spectra of adsorbed benzo[*b*]fluoranthene (Fig. 6) coincide for Si 22, 40 and 100 but exhibit a slight (6 nm) hypsochromic shift in Si 150.

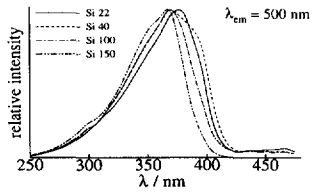

Fig. 3. Fluorescence excitation spectra of benzo[*b*]fluoranthene adsorbed on various silica gels at low surface coverages Θ_F (0.008–0.015).

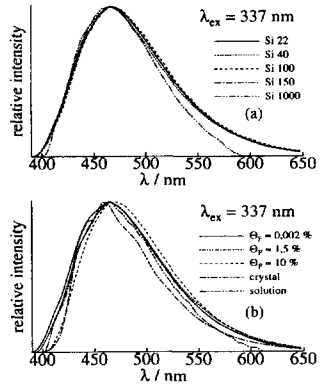

Fig. 4. Fluorescence spectra of fluoranthene adsorbed (a) on various silica gels at low surface coverages Θ_F (0.01–0.05) and (b) on Si 40 at various surface coverages Θ_F.

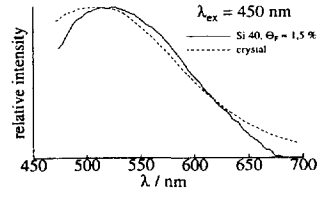

Fig. 5. Fluorescence spectra of adsorbed and crystalline fluoranthene upon excitation at 450 nm.

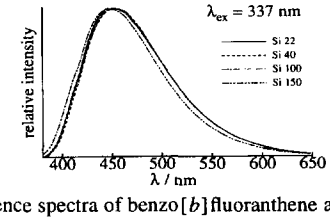

Fig. 6. Fluorescence spectra of benzo[*b*]fluoranthene adsorbed on various silica gels at low surface coverages Θ_F (0.008–0.015).

3.2. Fluorescence lifetimes

Generally decay curves followed first-order kinetics within the accuracy of determination. An example is reproduced in

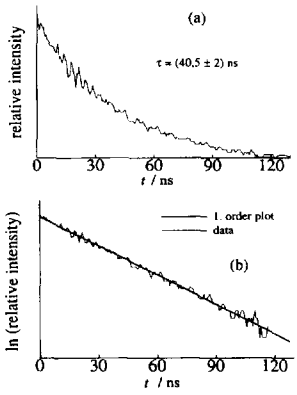

Fig. 7. (a) Fluorescence decay in vacuo of the fluorescence of fluoranthene adsorbed on Si 40. (b) Logarithmic plot of the data in (a) with the linear regression line.

Table 2
Lifetimes of fluoranthene fluorescence in the absence of quenchers (solid samples evacuated; solutions degassed by four freeze–pump–thaw cycles); values are the averages of at least ten measurements, and standard deviations are given

Environment	Covered surface fraction Θ_F	Lifetime τ (ns)
Fluoranthene		
Si 22	≤ 0.015	46 ± 1.5
Si 40	≈ 0.0002	44.5 ± 1.5
Si 40	≈ 0.015	47.5 ± 2.5
Si 40	≈ 0.10	40 ± 2
Si 100	≈ 0.035	45.5 ± 2.5
Si 150	≈ 0.045	46.5 ± 1.5
Si 1000	≈ 0.05	44.5 ± 1
Si 1000	≈ 0.50	24 ± 1
Solid crystals	–	27 ± 2
n-Heptane	–	47 [a]
Toluene	–	51 ± 2 [b]
Cyclohexane	–	53 [c]
Benzo[*b*]fluoranthene		
Si 22	≤ 0.008	48.5 ± 2.5
Si 40	≈ 0.008	50 ± 2
Si 100	≈ 0.012	48 ± 3.5
Si 150	≈ 0.015	47.5 ± 1
n-Heptane	–	44.3 [a]

[a] From [17], $c < 10^{-6}$ mol dm^{-3}.
[b] From [28].
[c] From [16], $c = 10^{-3}$ mol dm^{-3}.

Fig. 7. Fluorescence lifetimes in the absence of quenchers derived from such curves are given in Table 2 for fluoranthene and benzo[*b*]fluoranthene under various conditions. In order to allow the adsorbed molecules to find their equilibrium sites on the silica gel surface, the lifetimes were measured at least 1 week after the preparation of the sample. Lifetime values did not change upon repeating the experiments even after storing samples for more than one year. From inspection of the table it follows that (i) for both the molecules the lifetimes on silica gel and in diluted solution are similar while the fluorescence of a crystalline fluoranthene sample decays more rapidly and (ii) there is a dependence of the lifetime on the surface area Θ_F covered by fluoranthene.

3.3. Oxygen quenching

The fluorescence lifetimes and intensities were measured as functions of oxygen pressure. Spectra were not affected by the presence of oxygen. The lifetimes measured before the quenching experiments (Table 1) were reproducible after re-evacuation of samples. Quenching data are given in Fig. 8 in the form of Stern–Volmer plots according to the equation

$$\frac{I}{I_Q} = \frac{\tau}{\tau_Q} = \frac{\Phi}{\Phi_Q} = 1 + \tau k_q p(O_2) \qquad (1)$$

derived from intensity as well as from lifetime measurements for fluoranthene at various pore sizes. In Eq. (1), I is the fluorescence intensity, Φ the fluorescence quantum yield, τ the fluorescence lifetime, $p(O_2)$ the oxygen pressure and k_q the quenching constant; the suffix Q denotes the presence of quencher which is oxygen throughout. The figure shows that the quenching efficiency (expressed as I/I_Q or τ/τ_Q) increases with increasing pore size. In mesoporous gels (Si 40, 60, 100 and 150), however, the quenching efficiencies almost agree. Fig. 8 also reveals that there is a levelling off of the values as a function of oxygen pressure rather than a linear dependence as expected from Eq. (1). Only for the macroporous gel Si 1000 does the Stern–Volmer plot appear linear. Benzo[*b*]fluoranthene gives analogous results (Fig. 9).

In Figs. 10 and 11, Stern–Volmer plots for fluoranthene quenching at various surface coverages Θ_F are given. In mesoporous (Fig. 10) and macroporous (Fig. 11) gels, increasing surface coverage leads to reduced quenching efficiency. At a very low coverage (0.002%), however, this trend appears to be reversed.

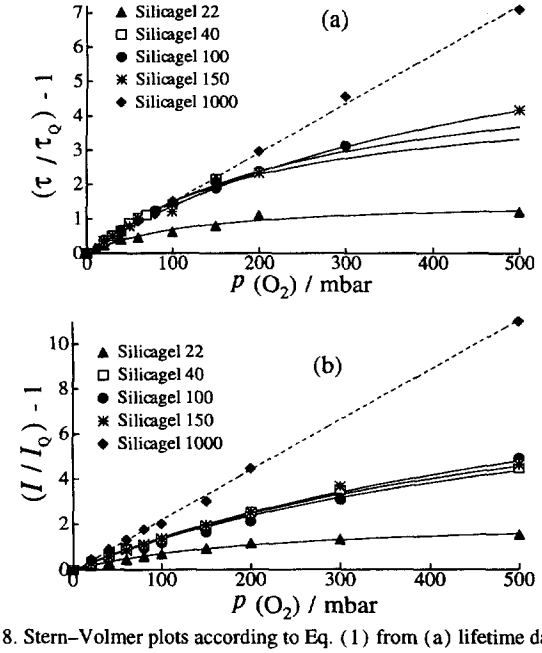

Fig. 8. Stern–Volmer plots according to Eq. (1) from (a) lifetime data and (b) intensity measurements of the fluorescence of fluoranthene adsorbed on various silica gels. The broken and full curves are plotted using Eq. (5)–(7); see text.

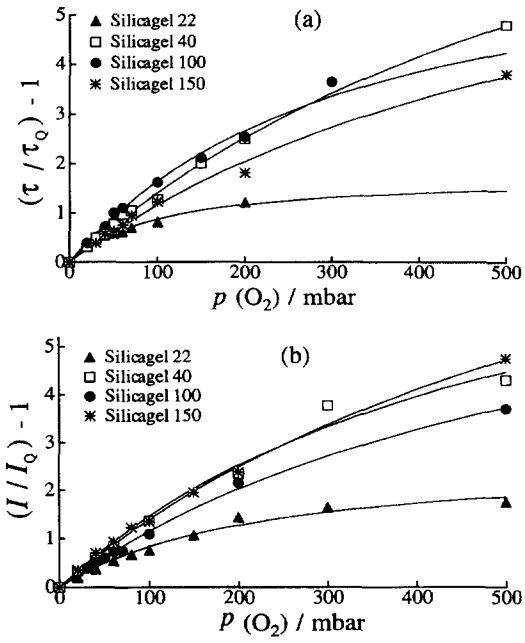

Fig. 9. Stern–Volmer plots according to Eq. (1) from (a) lifetime data and (b) intensity measurements of the fluorescence of benzo[*b*]fluoranthene adsorbed on various silica gels. The full curves are calculated from Eqs. (5)–(7); see text.

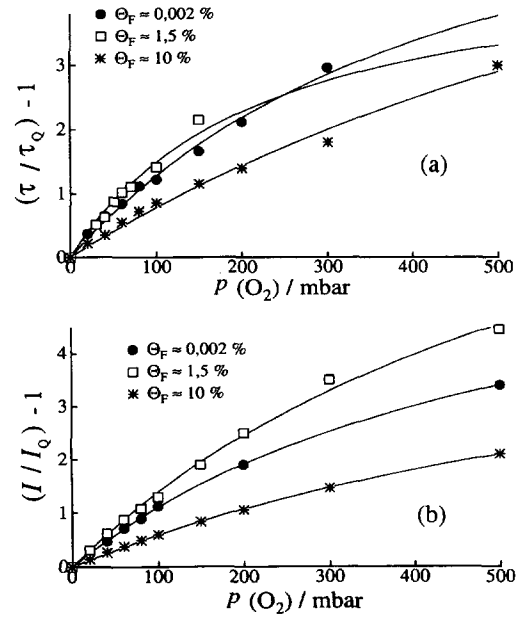

Fig. 10. Stern–Volmer plots according to Eq. (1) from (a) lifetime data and (b) intensity measurements of the fluorescence of fluoranthene adsorbed on Si 40 at various surface coverages Θ_F. The full curves are plotted using Eq. (5)–(7); see text.

3.4. Gas mixtures

Three photochemically inert gases were investigated: nitrogen, argon and carbon dioxide. The pure inert gases did not quench the fluorescence of fluoranthene and benzo[*b*]fluoranthene up to pressures of 1 bar. In mixtures with oxygen, interesting time-dependent phenomena were observed, depending on the series order of the addition of the

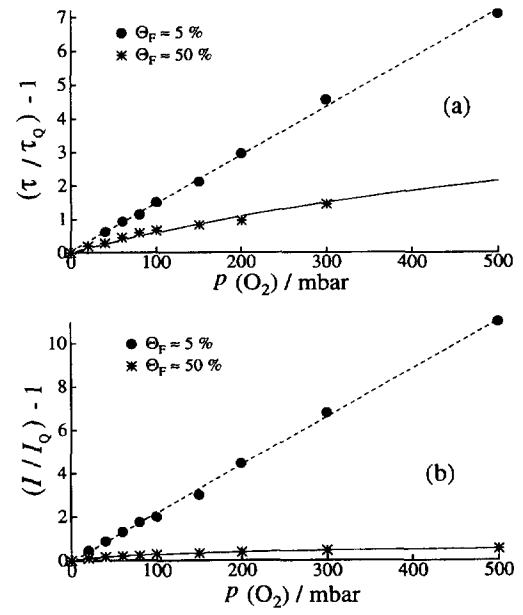

Fig. 11. Stern–Volmer plots according to Eq. (1) from (a) lifetime data and (b0 intensity measurements of the fluorescence of fluoranthene adsorbed on Si 1000 at two surface coverages Θ_F. The broken and full curves are plotted according to Eqs. (5)–(7); see text.

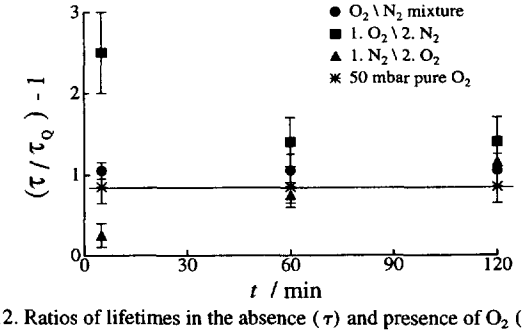

Fig. 12. Ratios of lifetimes in the absence (τ) and presence of O_2 (τ_Q), i.e. quenching efficiency, as a function of time t after the addition of gases.

gases to evaluated samples. These effects are illustrated in Fig. 12. In this figure the quenching efficiency of a reference system, pure oxygen at 50 mbar, did not change with time (horizontal line in Fig. 12). A slightly enhanced but time-independent efficiency of quenching is observed when separately mixed oxygen (50 mbar) and nitrogen (500 mbar) are added. When oxygen is added first and nitrogen thereafter, a considerable enhancement of quenching occurs, which after about 1 h approaches the value of the system containing premixed gases. When, however, nitrogen is added first and oxygen thereafter, an initial decrease in quenching efficiency takes place, which increases within the first hour after addition to reach the final value of the other two samples with gas mixtures. That is the eventual quenching efficiency is independent of the order of addition and slightly exceeds that for pure oxygen (as previously found for other fluorescent probes [9,10]). The described temporal behaviour qualitatively agrees for all three inert gases as well as for Si 40, Si 1000 and Si 22, the latter needing somewhat longer equilibration times. In Table 3, therefore, the ratios τ / τ_Q of the lifetime in

Table 3
Oxygen quenching efficiencies (lifetime divided by lifetime quenched) for fluoranthene and benzo[*b*]fluoranthene adsorbed on various silica gels at different surface coverages Θ in the presence of inert gases ($p(O_2) = 50$ mbar; $p(N_2, Ar, CO_2) = 500$ mbar); standard deviations are given

System	Θ	τ/τ_Q
Si 22–fluoranthene–O_2	$\leqslant 0.015$	1.55 ± 0.15
Si 22–fluoranthene–O_2–N_2	$\leqslant 0.015$	1.75 ± 0.15
Si 22–fluoranthene–O_2–Ar	$\leqslant 0.015$	1.80 ± 0.15
Si 22–fluoranthene–O_2–CO_2	$\leqslant 0.015$	1.65 ± 0.15
Si 40–fluoranthene–O_2	0.00002	1.70 ± 0.10
Si 40–fluoranthene–O_2–N_2	0.00002	1.95 ± 0.15
Si 40–fluoranthene–O_2–Ar	0.00002	1.85 ± 0.10
Si 40–fluoranthene–O_2–CO_2	0.00002	1.85 ± 0.15
Si 40–fluoranthene–O_2	0.015	1.85 ± 0.20
Si 40–fluoranthene–O_2–N_2	0.015	2.25 ± 0.25
Si 40–fluoranthene–O_2–Ar	0.015	2.15 ± 0.20
Si 40–fluoranthene–O_2–CO_2	0.015	2.05 ± 0.20
Si 40–fluoranthene–O_2	0.1	1.40 ± 0.10
Si 40–fluoranthene–O_2–N_2	0.1	1.45 ± 0.15
Si 40–fluoranthene–O_2–Ar	0.1	1.40 ± 0.20
Si 40–fluoranthene–O_2–CO_2	0.1	1.45 ± 0.20
Si 1000–fluoranthene–O_2	0.05	1.80 ± 0.10
Si 1000–fluoranthene–O_2–N_2	0.05	1.85 ± 0.25
Si 1000–fluoranthene–O_2–Ar	0.05	1.75 ± 0.20
Si 1000–fluoranthene–O_2–CO_2	0.05	1.85 ± 0.30
Si 22–benzo[*b*]fluoranthene–O_2	$\leqslant 0.008$	1.55 ± 0.15
Si 22–benzo[*b*]fluoranthene–O_2–N_2	$\leqslant 0.008$	1.60 ± 0.20
Si 22–benzo[*b*]fluoranthene–O_2–Ar	$\leqslant 0.008$	1.50 ± 0.20
Si 22–benzo[*b*]fluoranthene–O_2–CO_2	$\leqslant 0.008$	1.50 ± 0.20
Si 40–benzo[*b*]fluoranthene–O_2	0.008	1.90 ± 0.20
Si 40–benzo[*b*]fluoranthene–O_2–N_2	0.008	1.95 ± 0.15
Si 40–benzo[*b*]fluoranthene–O_2–Ar	0.008	2.00 ± 0.15
Si 40–benzo[*b*]fluoranthene–O_2–CO_2	0.008	1.90 ± 0.20

the absence to that in the presence of oxygen are listed for equilibrated systems, i.e. values measured at least 2 h after the gas addition. Inspection of the table reveals that quenching efficiencies increase with increasing pore size and decrease with increasing Θ_F, except for very low surface coverage on Si 40 (as in the absence of inert gases), and that the presence of inert gases increases the efficiency slightly.

4. Discussion

4.1. Spectra

When excitation spectra at almost constant low surface coverages ($\Theta \leqslant 0.05$) are compared (Fig. 2(a)), a dependence on pore size becomes obvious. In the macroporous Si 1000 the spectrum is not very different from that of a monomeric fluoranthene in dilute solution. The observed red shift upon decreasing the pore size points to the formation of J-aggregates, i.e. head-to-tail aggregates [34,35]. We can be quite sure that these aggregates are equilibrium states formed after adsorption of monomers rather than artefacts of the preparation since (i) the spectra remain unchanged when stored for 1 year, (ii) the peaks in the monomer spectrum are not observable once the aggregates are present (Fig. 2) and (iii) a different preparation method [1] leads to identical results. A prerequisite for the formation of aggregates is motion of aromatic molecules on silica gel surfaces, which is known to occur [36,37]. This motion, on the contrary, would allow the aggregates to disjoin and form a system of adsorbed monomers, if this was the thermodynamically stable situation. In accordance with the above interpretation, ground-state aggregates grow with increasing surface coverage as indicated by the extending red shift.

In spite of the fact that the excitation spectra exhibit aggregate formation, in the emission spectra monomer fluorescence predominates by far (upon excitation at 337 nm, which is also the wavelength of excitation for the time-resolved measurements). This in connection with the observed strict first-order decay kinetics means that, upon excitation of the aggregates, excited monomers are released which can emit fluorescence. This takes place as long as the excitation energy is sufficient to excite monomers, while low energy excitation results in an excimer-like emission (Fig. 5).

4.2. Decay curves

The small portion of excimer emission, which appears in the long-wavelength tails of the spectra (Fig. 4(a)), obviously does not measurably affect the decay profile (which integrates the whole spectrum), since first-order kinetics are observed throughout. Thus a single species must be the emit-

ter, and possible sites of the adsorbed molecules must be very similar. These features of the system are fortunate for quenching studies and are possibly a consequence of our drying procedure which results in a homogeneous surface consisting of vicinal and geminal silanol groups [25].

4.3. Quenching mechanism

Since photochemical reactions of fluoranthene and benzo[*b*]fluoranthene were not observed, we can attribute the reduced lifetimes and fluorescence intensities upon addition of oxygen to fluorescence quenching. Except for Si 1000, Fig. 8–10 clearly exhibit saturation phenomena. The Eley–Rideal mechanism is therefore impossible, since it requires a proportionality of quenching efficiency and oxygen pressure. Also, the obvious dependence of the quenching on pore size disagrees with quenching from the gas phase exclusively.

When, instead, the alternative Langmuir–Hinshelwood mechanism is operative, we have to expect a proportionality of quenching efficiency and the area Θ_O of the surface covered by oxygen, so that Eq. (1) is modified to

$$\frac{I}{I_Q} = \frac{\tau}{\tau_Q} = \frac{\Phi}{\Phi_Q} = 1 + \tau k_Q \Theta_O \tag{2}$$

with Θ_O defined as

$$\Theta_O = \frac{K(O_2)p(O_2)}{1 + K(O_2)p(O_2)} \tag{3}$$

where $K(O_2)$ is the equilibrium constant of adsorption and desorption:

$$K(O_2) = \frac{k_a(O_2)}{k_b(O_2)} \tag{4}$$

By substitution, Eq. (2) becomes

$$\frac{\tau}{\tau_Q} = 1 + \frac{\tau k_Q K(O_2)p(O_2)}{1 + K(O_2)p(O_2)} \tag{5}$$

and after linearization we have

$$\frac{\tau \cdot \tau_Q}{\tau - \tau_Q} = \frac{1}{k_Q K(O_2)} \frac{1}{p(O_2)} + \frac{1}{k_Q} \tag{6}$$

or for steady-state intensity data

$$\frac{\tau I_Q}{I - I_Q} = \frac{1}{k_Q K(O_2)} \frac{1}{p(O_2)} + \frac{1}{k_Q} \tag{7}$$

Plots according to Eq. (6) and Eq. (7) respectively indeed reveal a linear relationship proving the Langmuir–Hinshelwood mechanism, as shown by the examples in Fig. 13. The intersections of such plots with the *y* axis yield values for k_Q, which are listed in Table 4. Values derived from time-resolved and steady-state measurements respectively agree within error limits but the latter always exceed the former, indicating some systematic difference in the two methods. Eqs. (5)–(7) were also used to fit the data in Figs. 8–11 as indicated by the full lines resembling the measured points

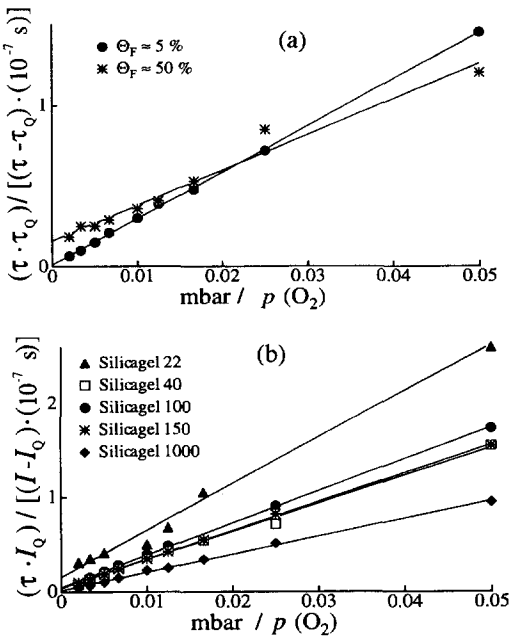

Fig. 13. Examples for plots according to the linearized Langmuir–Hinshelwood Eqs. (6) and (7): (a) data from Fig. 11(a); (b) data from Fig. 8(b).

and by the broken curves in the case of Si 1000. Since saturation is not reached in the latter gel, the data might be fitted by the Stern–Volmer equation as well, so that the Eley–Rideal mechanism cannot be excluded in this case.

Further evaluation of the data eventually delivers heats of adsorption for oxygen on the respective silica gel preparation: from the slope of straight lines such as shown in Fig. 13 we can obtain $K(O_2)$; further, k_a can be calculated from gas theory according to

$$k_a = 2 \frac{r_O}{(2\pi m_O k_B T)^{1/2}} \tag{8}$$

and $k_d = k_a / K(O_2)$ is related to the heat Q of adsorption:

$$k_d = \nu_d \exp\left(-\frac{Q}{RT}\right) \tag{9}$$

With r_O being the van der Waals radius and m_O the mass of an oxygen molecule, we obtain, at 295 K, $k_a(O_2) = 3.54 \times 10^5$ mbar^{-1} s^{-1}. ν_d is a fundamental frequency of the adsorbed molecule assumed to be 10^{13} s^{-1}. With these numbers, Q assumes the values listed in Table 4. The values obtained are in the range expected for physical adsorption. (For N_2 and Ar on silica gel, adsorption heats between 15 and 20 kJ mol^{-1} at room temperature can be found in the literature [38–40].) From inspection of the table it follows that Q assumes higher values in materials with narrow pores (at Θ_F almost constant between 0.008 and 0.05). Qualitatively the same dependence on pore size for heats of adsorption is known from independent experiments in zeolites [41].

At almost constant low surface coverage Θ_F (between 0.008 and 0.05) the quenching constants listed in Table 4 increase with increasing pore size, i.e. by a factor of 4 when changing from the microporous Si 22 to mesoporous systems,

Table 4
Quenching constants k_Q derived from linearized Langmuir–Hinshelwood plots according to Eq. (6) and Eq. (7) with linear correlation coefficients r and heats of oxygen adsorption on the respective silica gel preparations calculated from Eq. (9); for k_Q and Q the error limits from least-squares and error propagation analysis are given

System	Θ_F	k_Q ($\times 10^7$ s^{-1})	r	Q (kJ mol^{-1})
From τ/τ_0				
Si 22–fluoranthene	≤ 0.015	2.5 ± 1	0.996	31.5 ± 1.5
Si 40–fluoranthene	0.00002	8.5 ± 3.5	0.997	29 ± 1.5
Si 40–fluoranthene	0.015	19 ± 8	0.995	26.5 ± 1.5
Si 40–fluoranthene	0.1	9 ± 3.5	0.996	28 ± 1.5
Si 100–fluoranthene	0.035	13 ± 5	0.996	27.5 ± 1.5
Si 150–fluoranthene	0.045	13 ± 5	0.998	28 ± 1.5
Si 1000–fluoranthene	0.05	95 ± 40	0.999	24 ± 1.5
From I/I_0				
Si 22–fluoranthene	≤ 0.015	5 ± 2	0.999	29 ± 1.5
Si 40–fluoranthene	0.00002	11 ± 4.5	0.999	27.5 ± 1.5
Si 40–fluoranthene	0.015	23 ± 9	0.999	26 ± 1.5
Si 40–fluoranthene	0.1	9.5 ± 3.5	0.999	27 ± 1.5
Si 100–fluoranthene	0.05	22 ± 9	0.999	26 ± 1.5
Si 150–fluoranthene	0.05	26 ± 10	0.999	25.5 ± 1.5
Si 1000–fluoranthene	0.05	70 ± 30	0.999	24.5 ± 1.5
Si 1000–fluoranthene	0.5	2.5 ± 1	0.994	30 ± 1.5
From τ/τ_0				
Si 22–benzo[b]fluoranthene	≤ 0.008	2.5 ± 1	0.992	31.5 ± 1.5
Si 40–benzo[b]fluoranthene	0.008	17 ± 7	0.997	26.5 ± 1.5
Si 100–benzo[b]fluoranthene	0.012	17 ± 7	0.998	26.5 ± 1.5
Si 150–benzo[b]fluoranthene	0.015	15 ± 6	0.998	27.5 ± 1.5
From I/I_0				
Si 22–benzo[b]fluoranthene	≤ 0.008	5 ± 2	0.999	29 ± 1.5
Si 40–benzo[b]fluoranthene	0.008	12 ± 5	0.996	27.5 ± 1.5
Si 100–benzo[b]fluoranthene	0.012	13 ± 5	0.995	27 ± 1.5
Si 150–benzo[b]fluoranthene	0.015	14 ± 6	0.999	27.5 ± 1.5

and by a factor of 15 in the macroporous Si 1000. The same trend was found by Drake et al. [9,10] and Wellner et al. [9,12] when changing from mesoporous to macroporous gels. Among the mesoporous gels there is no significant difference in k_Q, as found previously for anthracene quenching on Si 60 and Si 100 [7]. This may originate from the fact that there is a comparatively wide pore size distribution in the commercial mesoporous silica gels (as revealed from data sheets of the suppliers; cf. Table 1). For fluoranthene on a synthetic silica gel of uniform pore size (3.5 nm), however, values corresponding to between Si 22 and Si 40 were found ($k_Q = 10$ s^{-1}; $Q = 27$ kJ mol^{-1} [1]). We can rationalize the pore size dependence of k_Q by considering the increased heat of adsorption in narrow pores (which should hold for the adsorbed fluoranthenes as well). This leads to a reduced translational mobility of the reaction partners on the surface and thus slows down the quenching rate constant. Reduced mobilities in narrow pores were independently found in energy transfer and excimer formation experiments respectively [42,43].

Three experiments using Si 40 were performed in order to investigate the dependence of the rate constant of fluorescence quenching on the area Θ_F covered by fluoranthene. It turned out that k_Q passes through a maximum. The increase in k_Q from very low to intermediate (a few per cent) coverages is in keeping with the general observation that translational mobilities on surfaces increase with Θ independent of whether only one sort of molecule or mixtures are adsorbed [44–47]. This rise in mobility was rationalized in terms of adsorbates sliding over coadsorbed molecules, the adsorption forces being reduced thereby. A reason for the decrease in k_Q at very high Θ_F may arise from the aggregation phenomena discussed above; excited molecules inside an aggregate or cluster of fluoranthene may be protected from oxygen, i.e. the necessary encounter complex of oxygen and excited fluoranthene (cf. [48]) cannot be formed.

4.4. Inert gases

The observed dependence of quenching efficiency on the order of gas addition cannot be a consequence of initial incomplete mixing in the gas phase which is quite fast, since it is brought about by interpenetration due to pressure differences rather than by molecular diffusion. Inside the pores the transport of molecules is considerably slower, since under the experimental conditions the mean free distance between gas molecules exceeds the pore radius (Knudsen range [49]). Diffusion constants therefore become much smaller

[50]. Slow mixing inside pores, however, cannot be the only reason for the observed effects, since in that case the time needed to reach equilibration should shorten in macroporous gels which contradicts the results. Therefore we propose opposing effects of the coadsorption of gases to be responsible for the observations. On the one hand, coadsorption increases the mobility of oxygen, leading to the initially enhanced quenching rate when oxygen is adsorbed first. On the other hand, equilibration reduces the surface area covered by oxygen in the presence of inert gases according to

$$\Theta_O = \frac{K(O_2)p(O_2)}{1+K(O_2)p(O_2)+K(I)p(I)} \quad (10)$$

where $K(I)$ and $p(I)$ refer to inert gases. The fact that in all cases after equilibration an eventual small increase in quenching efficiency is observed means that the former effect somewhat exceeds the latter. In the case of primarily adsorbed N_2, adsorption sites are occupied by the inert gas initially, so that the quenching efficiency increases until the equilibrium (10) is reached.

5. Conclusion and outlook

Oxygen quenching of fluoranthene and benzo[*b*]fluoranthene adsorbed on silica gels is well described by the Langmuir–Hinshelwood mechanism. A method for determining heats of adsorption from fluorescence quenching is opened, which should be applicable to all quenching gases. For more accurate data the pre-exponential factor ν_d in Eq. (9) must be determined exactly from measurements at different temperatures. In applications of such systems to oxygen sensors the non-linear dependence of quenching on oxygen pressure and the slow equilibration upon mixing of gases have to be considered.

Acknowledgements

This work is a project of the Graduiertenkolleg "Chemische Reaktivität und Molekulare Ordnung" supported by the Deutsche Forschungsgemeinschaft and by the Minister für Wissenschaft und Forschung des Landes Nordrhein-Westfalen. The financial assistance of the Fonds der Chemischen Industrie is gratefully acknowledged.

References

[1] C. Springob, G. von Bünau, T. Wolff and F. Schüth, *Ber. Bunsenges. Phys. Chem., 100* (1996) 1206.
[2] H. Kautsky and H. de Bruijn, *Naturwissenschaften, 19* (1931) 1043.
[3] H. Kautsky, H. de Bruijn, R. Neuwirth and W. Baumeister, *Chem. Ber., 66* (1933) 158.
[4] D. Oelkrug, W. Flemming, R. Füllemann, R. Günther, W. Honnen, G. Krabichler, M. Schäfer and S. Uhl, *Pure Appl. Chem., 58* (1986) 1207.
[5] A.J. Twarowski and L. Good, *J. Phys. Chem., 91* (1987) 5252.
[6] R. Krasnansky, K. Koike and J.K. Thomas, *J. Phys. Chem., 94* (1990) 4521.
[7] T. Wolff, F. Akbarian and G. von Bünau, *Ber. Bunsenges. Phys. Chem., 94* (1990) 833.
[8] V.V. Osipov, A.Y. Ritter and V.N. Yankvich, *Russ. J. Phys. Chem., 65* (1991) 227.
[9] J.M. Drake, P. Levitz, J. Klafter, N.J. Turro, J.S. Nitsche and K.F. Cassidy, *Phys. Rev. Lett., 61* (1988) 865.
[10] J.M. Drake, P. Levitz, N.J. Turro, K.S. Hitsche and K.F. Cassidy, *J. Phys. Chem., 92* (1988) 4680.
[11] J. Samuel, M. Ottolenghi and D. Avnir, *J. Phys. Chem., 96* (1992) 6398.
[12] E. Wellner, D. Rojanski, M. Ottolenghi, D. Huppert and D. Avnir, *J. Am. Chem. Soc., 109* (1987) 575.
[13] O.S. Wolfbeis and G. Boisde, in W. Göpel, J. Hesse and J.N. Zemel (eds.), *Sensors. A Comprehensive Survey*, Vol. 3, VCH, Weinheim, 1992, pp. 893ff.
[14] W. Trettnak, in O.S. Wolfbeis (ed.), *Fluorescence Spectroscopy. New Methods and Applications*, Springer, Berlin, 1993, pp. 81ff.
[15] O.S. Wolfbeis, *Nachr. Chem. Tech. Lab., 43* (1995) 313.
[16] I.B. Berlman, H.O. Wirth and O.J. Steingraber, *J. Am. Chem. Soc., 90* (1968) 566.
[17] H. Güsten and G. Heinrich, *J. Photochem., 18* (1982) 9.
[18] C. Grewer, C. Wirp, M. Neumann and H.-D. Brauer, *Ber. Bunsenges. Phys. Chem., 98* (1994) 997.
[19] K. Kikuchi, *Chem. Phys. Lett., 183* (1991) 103.
[20] L. Yip, J.B. Hudson and G.H.N. Towers, *Planta Med., 61* (1995) 187.
[21] D.L. Philen and R.M. Hedges, *Chem. Phys. Lett., 43* (1976) 358.
[22] R.V. Nauman, H.E. Holloway and J.H. Wharton, *Chem. Phys. Lett., 122* (1985) 523.
[23] K.-M. Bark and R.K. Force, *J. Phys. Chem., 93* (1989) 7985.
[24] R.K. Iller, *The Chemistry of Silica: Solubility, Polymerization, Colloid and Surface Properties, and Biochemistry*, Wiley, New York, 1978, p. 625.
[25] Y.S. Liu, P. de Mayo, W.R. Ware, *J. Phys. Chem., 97* (1993) 5987.
[26] T. Wolff, K. Pfanner and C. Springob, *J. Photochem. Photobiol. A: Chem., 74* (1993) 247.
[27] J.N. Demas, *Excited State Lifetime Measurements*, Academic Press, London, 1982, p. 234.
[28] I.B. Berlman, *Handbook of Fluorescence Spectra of Organic Molecules*, 2nd edn., Academic Press, New York, 1971, p. 364.
[29] R. Dunsbach and R. Schmidt, *J. Photochem. Photobiol. A: Chem., 83* (1994) 7.
[30] H.H. Perkampus, *Z. Phys. Chem. (Wiesbaden), 13* (1957) 278.
[31] B. Stevens, *Spectrochim. Acta, 18* (1962) 439.
[32] D. Oelkrug, M. Radjaipour and H. Erbse, *Z. Phys. Chem. (Wiesbaden), 88* (1974) 23.
[33] T. Förster, *Angew. Chem., 81* (1969) 364.
[34] A.H. Herz, *Photogr. Sci. Eng., 18* (1974) 323.
[35] M. Pope and C.E. Swenberg, *Electronic Processes in Organic Crystals*, Oxford University Press, Oxford, 1982, p. 43.
[30] P. DeMayo, K. Okada, M. Rafalska, A.C. Weedon and G.S.K. Wong, *J. Chem. Soc., Chem. Commun.*, (1981) 820.
[37] D. Avnir, L.J. Johnston, P. DeMayo and S.K. Wong, *J. Chem. Soc., Chem. Commun.*, (1981) 958.
[38] B.G. Aristov and A.V. Kiselev, *Russ. J. Phys. Chem., 38* (1964) 1077.
[39] M.R. Bhambhani, P.A. Cutting, K.S.W. Sing and D.H. Turk, *J. Colloid Interface Sci., 38* (1972) 109.
[40] T.P. Bebe, Jr. and J.T. Yates, Jr., *Surf. Sci., 159* (1985) 369.
[41] H. Stach, U. Lohse, H. Thamm and W. Schirm, *Zeolites, 6* (1986) 74.
[42] S. Yamamura, Y. Tatsu, S. Yoshikawa and T. Yazawa, *J. Photochem. Photobiol. A: Chem., 63* (1992) 87.
[43] C.R. Roxlo, P. Mitra, H.W. Deckmann, D. Abeles and P.P. Wong, *Materials Research Society Symposium Proceedings*, Vol. 76, Materials Research Society, Pittsburgh, PA, 1987, p. 31.
[44] R. Haul and K. Hübner, *Ber. Bunsenges. Phys. Chem., 79* (1985) 777.

[45] P. DeMayo, L.V. Natarajan and W.R. Ware, *J. Phys. Chem., 89* (1985) 3526.
[46] D. Avnir, R. Busse, M. Ottolenghi, E. Wellner and K.A. Zachariasse, *J. Phys. Chem., 89* (1985) 3521.
[47] T. Fujii, A. Ishii, H. Satozono, S. Suzuki, N. Takusagawa and M. Anpo, *J. Photochem. Photobiol. A: Chem., 84* (1994) 283.
[48] C. Grewer, C. Wirp, M. Neumann and H.-D. Brauer, *Ber. Bunsenges. Phys. Chem., 98* (1994) 997.
[49] J. Kärger and M.D. Ruven, *Diffusion in Zeolites and Other Microporous Solids,* Wiley, New York, 1992, p. 98.
[50] R.B. Evans, G.M. Watson and E.A. Mason, *J. Phys. Chem., 65* (1961) 2076.